

Ligand Structural Effects on the Electrochemistry of Chromium(III) Amino Carboxylate Complexes

Mathias Hecht[†]

Fachbereich Informatik, Mathematik und Naturwissenschaften, Hochschule für Technik, Wirtschaft und Kultur, Postfach 66, Leipzig D-04251, Germany

Franklin A. Schultz*

Department of Chemistry, Indiana University-Purdue University at Indianapolis, 402 North Blackford Street, Indianapolis, Indiana 46202-3274

Bernd Speiser*

Institut für Organische Chemie, Universität Tübingen, Auf der Morgenstelle 18, D-72076 Tübingen, Germany

Received February 9, 1996[⊗]

The aqueous electrochemical behavior of 10 Cr(III) complexes with potentially tri- and hexadentate amino carboxylate ligands is reported and is shown to depend on the composition and spatial arrangement of the donor atom set. Complexes with two amine and four carboxylate donors (N_2O_4) and two amine, one aquo, and three carboxylate donors (N_2O_3O') in which the N atoms are coordinated *cis* to one another undergo chemically and electrochemically reversible reduction at ca. -1.4 and ca. -1.2 V vs SCE, respectively. However, complexes with a *trans*- N_2O_4 donor atom set, as exemplified by $Cr(MIDA)_2^-$ ($MIDA^{2-} = N$ -methyliminodiacetate), undergo quasi-reversible $Cr^{III/II}$ reduction at ca. -1.4 V that is followed by a sequence of reactions which establishes an electrochemical square scheme. The chemical reactions in the scheme involve displacement of a bound carboxylate group following reduction to Cr(II) and its reattachment after reoxidation to Cr(III). This mechanistic sequence is analyzed by digital simulation, and values of formal potentials, transfer coefficients, and chemical and electrochemical rate constants are reported for $Cr(MIDA)_2^-$ and its *N*-ethyl homolog. The difference in electrochemical behavior between *cis*- and *trans*- N_2O_4 complexes is attributed to differences in the Jahn–Teller distortions experienced by these structures upon reduction to Cr(II). It is proposed that simultaneous N–Cr–N bond elongation, which is possible only for *trans* species, leads to greater strain in the facially coordinated *N*-alkyliminodiacetate ligand and thus increases the barrier to electron transfer and facilitates Cr–carboxylate bond cleavage after reduction.

Introduction

The chromium(III/II) couple generally exhibits slow electron transfer kinetics in the presence of weak-field ligands.¹ This is thought to be a consequence of the large inner-shell reorganizations that accompany creation of the Jahn–Teller distorted coordination environment in high-spin Cr(II).² Small values of the heterogeneous electrochemical ($k_{s,h}$) and homogeneous (k_{ex}) electron self-exchange rate constants for $Cr(H_2O)_6^{3+/2+}$ ($k_{s,h} = 3 \times 10^{-6} \text{ cm s}^{-1}$,³ $k_{ex} \leq 2.0 \times 10^{-5} \text{ M}^{-1} \text{ s}^{-1}$)⁴ are explicable on this basis. However, the $Cr^{III/II}$ –EDTA couple exhibits considerably more facile electron transfer

kinetics ($k_{s,h} = 0.45 \text{ cm s}^{-1}$,⁵ $k_{ex} = 3 \times 10^3 \text{ M}^{-1} \text{ s}^{-1}$)⁶ and therefore is surprising in this regard.

This paper reports the kinetics and mechanism of electrochemical reduction of chromium(III) complexes with amino carboxylate ligands. Our interest in these compounds began with the discovery that the *cis*-bis(iminodiacetato) and *trans*-bis(*N*-methyliminodiacetato) complexes of Cr^{III} exhibit dramatically different electrochemical behaviors. This was reported in a preliminary manner in ref 7. However, full understanding of the phenomenon required examination of a larger number of complexes; thus, our investigation expanded to include the amino carboxylate ligands shown in Chart 1. These molecules provide the coordination environments illustrated in Chart 2. Included therein are complexes having two amine and four carboxylate donors bound to the metal with the amine nitrogens located *cis* [*cis*- N_2O_4 (A), *cis*- N_2O_4 (B)] or *trans* (*trans*- N_2O_4) to one another as well as those in which one carboxylate donor

[†] Present address: Department of Chemistry, University of California, Davis, CA 95616.

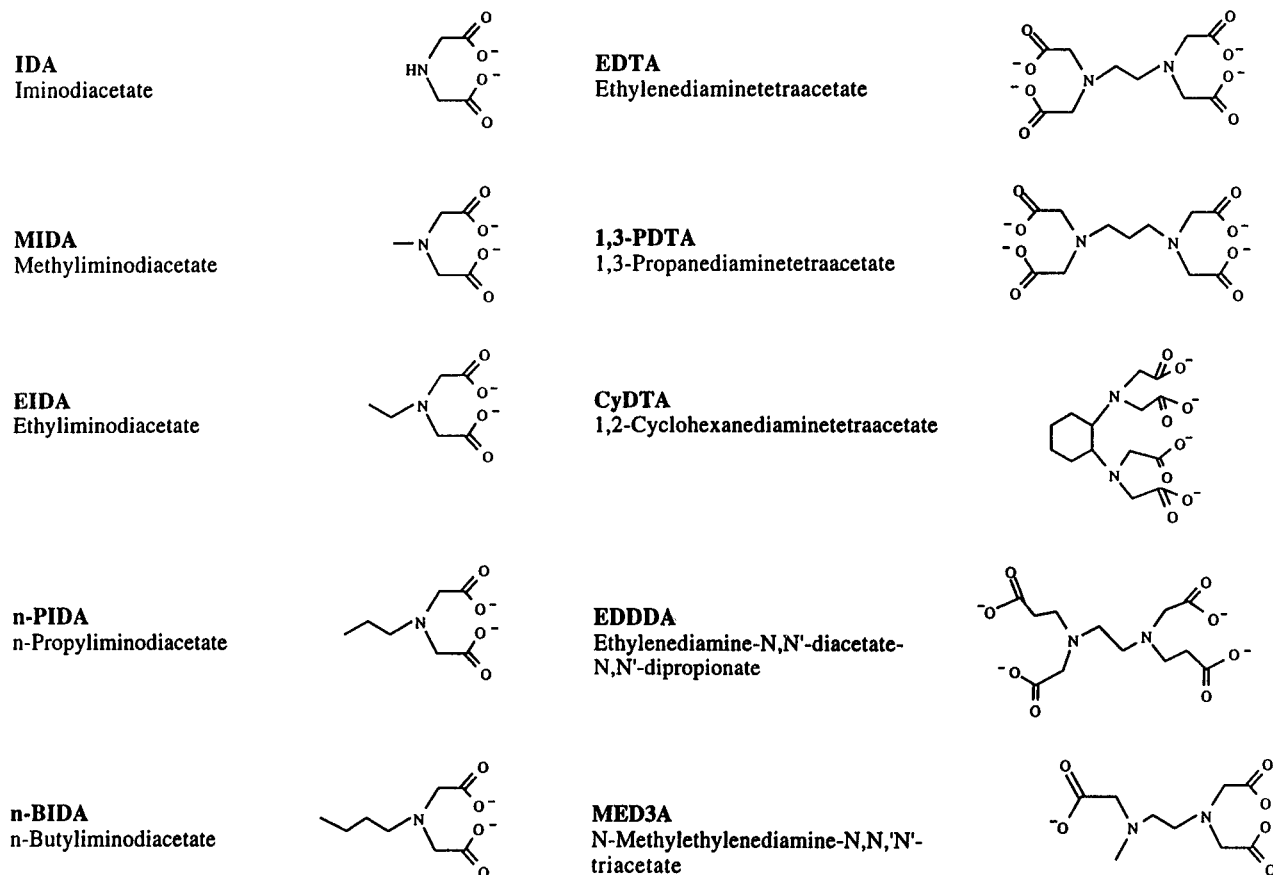
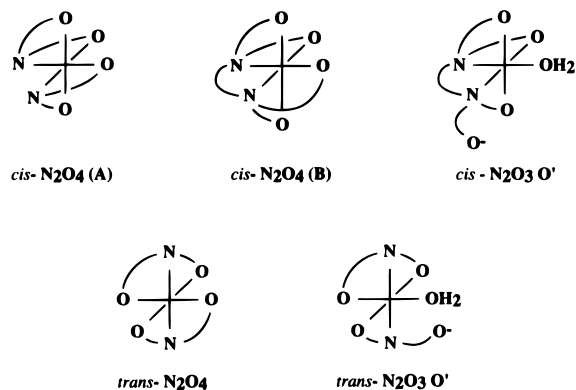
[⊗] Abstract published in *Advance ACS Abstracts*, August 15, 1996.

- (1) (a) Larkworthy, L. F.; Nolan, K. B.; O'Brien, P. In *Comprehensive Coordination Chemistry*; Wilkinson, G., Gillard, R. D., McCleverty, J. A., Eds.; Pergamon Press: Oxford, U.K., 1987; Vol. 3, pp 699–969. (b) Wilkins, R. G. *Kinetics and Mechanism of Reaction of Transition Metal Complexes*, 2nd ed.; VCH Publishers: New York, 1991.
- (2) (a) Bersuker, I. B. *Coord. Chem. Rev.* **1975**, *14*, 357. (b) Bersuker, I. B. *The Jahn–Teller Effect and Vibronic Interactions in Modern Chemistry*; Plenum Press: New York, 1984.
- (3) Hupp, J. T.; Weaver, M. J. *J. Phys. Chem.* **1984**, *88*, 6128.
- (4) Anderson, A.; Bonner, N. A. *J. Am. Chem. Soc.* **1954**, *76*, 3826.

(5) Zhang, X.; Yang, H.; Bard A. J. *J. Am. Chem. Soc.* **1987**, *109*, 1916.

(6) Wilkins, R. G.; Yelin, R. E. *Inorg. Chem.* **1968**, *7*, 2667.

(7) Meier, R.; Boddin, M.; Hecht, M.; Schultz, F. A. In *Molecular Electrochemistry of Inorganic, Bioinorganic and Organometallic Compounds*; Pombeiro, A. J. L., McCleverty, J. A., Eds.; NATO ASI Series C; Kluwer: Dordrecht, The Netherlands, 1993; Vol. 385, pp 489–494.

Chart 1. Structures and Abbreviations of Amino Carboxylate Ligands**Chart 2.** Amino Carboxylate Coordination Environments

has been replaced by water (*cis*-N₂O₃O' and *trans*-N₂O₃O'). On the basis of an examination of compounds with these structures, we present a more complete description of the electrode reaction mechanism of Cr^{III}(MIDA)₂⁻ and its higher *n*-alkyl homologs and an interpretation of the influence of coordination environment on Cr^{III/II} amino carboxylate electrochemistry.

Experimental Section

Materials. The ligands H₂MIDA, Na₂IDA·H₂O, H₄-1,3-PDTA, H₄-EDDDA·3H₂O, Na₂H₂EDTA·2H₂O, and H₄CyDTA·H₂O were purchased commercially in the purest form available and used as received. H₂EIDA was prepared according to Uehara et al.⁸ and recrystallized three times from ethanol/water. H₂-*n*-PIDA and H₂-*n*-BIDA were prepared as described by Stein et al.⁹ The complexes Na[Cr(MIDA)₂]₂¹⁰

K[Cr(EIDA)₂]₂,^{11a} K[Cr(*n*-PIDA)₂]₂,^{11a} K[Cr(*n*-BIDA)₂]₂,^{11a} K[Cr-(IDA)₂]₂·2.5H₂O,¹⁰ Na[Cr(1,3-PDTA)]₂·3H₂O,¹⁰ K[Cr(EDDDA)]₂,¹² [Cr-(HEDTA)(H₂O)]₂,¹³ and Na[Cr(CyDTA)(H₂O)]₂·3H₂O¹⁴ were synthesized by literature methods.

Solutions of chromium(III) complexes were prepared determinately from the above compounds using doubly distilled water. Unless otherwise stated, solutions examined in electrochemical experiments also contained 0.1 M ligand and were adjusted to an ionic strength of 1.0 M with Na₂SO₄ at pH 8.50. Oxygen was removed by deaeration with argon gas.

Electrochemical Experiments. Electrochemical experiments were performed in Germany with a BAS 100B potentiostat and in the United States with an EG&G PAR 173/179 potentiostat. A three-electrode electrochemical cell was used in all cases. The working electrode was an EG&G PAR Model 303A or a Metrohm Model EA290 stationary Hg drop electrode. The reference electrode was either a saturated calomel electrode (SCE) or an Ag/AgCl (saturated KCl) electrode (SE) whose potential is 0.199 V versus NHE. All potentials are reported versus the SCE. Compensation of solution resistance was accomplished mathematically by adaptation of the method of Imbeaux et al.¹⁵

Simulations. Simulation of cyclic voltammetric responses was performed with the program CVSIM,¹⁶ which is based on the use of orthogonal collocation¹⁷⁻¹⁹ to spatially discretize the reaction-diffusion equations of electrode reaction mechanisms. Several improvements have been made over the original numerical formulations to provide

(8) Uehara, A.; Kyuno, E.; Tsuchiya, R. *Bull. Chem. Soc. Jpn.* **1970**, *43*, 1394.
 (9) Stein, A.; Gregor, H. P.; Spoerri, P. E. *J. Am. Chem. Soc.* **1955**, *77*, 191.

(10) Weyh, J. A.; Hamm, R. E. *Inorg. Chem.* **1968**, *7*, 2431.
 (11) (a) Wernicke, R.; Schmidtke, H.-H.; Hoggard, P. E. *Inorg. Chim. Acta* **1977**, *24*, 145. (b) Hoggard, P. E.; Schmidtke, H.-H. *Ber. Bunsen-Ges. Phys. Chem.* **1972**, *76*, 1013.
 (12) Radanovic, D. J.; Douglas, B. E. *J. Coord. Chem.* **1975**, *4*, 191.
 (13) Hamm, R. E. *J. Am. Chem. Soc.* **1953**, *75*, 5670.
 (14) Tanaka, N.; Kanno, K.; Tomita, T.; Yamada, A. *Inorg. Nucl. Chem. Lett.* **1971**, *7*, 953.
 (15) (a) Imbeaux, J. C.; Saveant, J. M. *J. Electroanal. Chem. Interfacial Electrochem.* **1970**, *28*, 325. (b) Hecht, M. Ph.D. Thesis, Leipzig University, 1990.
 (16) Speiser, B. *Comput. Chem.* **1990**, *14*, 127.

Table 1. Spectroscopic and Electrochemical Data for Chromium(III) Amino Carboxylate Complexes

ligand	λ_{\max} , nm (ϵ , $M^{-1} \text{ cm}^{-1}$)				ref	$E_1^{\circ'}$, V (ΔE_p , mV) ^a	$E_2^{\circ'}$, V (ΔE_p , mV) ^a
	this work		lit.				
	<i>trans</i> -CrN ₂ O ₄						
MIDA	494 (38)	361 (26)	495 (42)	362 (29)	10	-1.466 (120) ^b	-1.209 ^c
EIDA	501 (38)	363 (29)	504 (36)	363 (24)	8	-1.380 (105) ^b	-1.173 ^c
<i>n</i> -PIDA	502 (41)	361 (27)	500	360	11	-1.383 (113) ^b	-1.190 ^c
<i>n</i> -BIDA	502 (43)	362 (29)	508	361	11	-1.350 (96) ^b	-1.166 ^c
	<i>cis</i> -CrN ₂ O ₄						
IDA	527 (74)	391 (83)	519 (76)	391 (79)	10	-1.394 (65)	
1,3-PDTA	506 (116)	382 (83)	509 (118)	385 (73)	10	-1.346 (62) ^d	
EDDDA	528 (198)	394 (102)				-1.428 (68) ^e	
	<i>cis</i> -CrN ₂ O ₃ O'						
MED3A			539 (143)	386 (113)	35		-1.243 (67) ^f
EDTA	540 (204)	390 (113)	540 (205)	390 (117)	33a		-1.238 (64) ^e
CyDTA	542 (204)	390 (97)	548 (215)	394 (103)	14		-1.192 (65) ^e

^a Obtained by cyclic voltammetry at a scan rate of 0.1 V s⁻¹ under conditions of 1 mM complex, 0.1 M excess ligand, $\mu = 0.1 \text{ M}$ (Na_2SO_4), and pH 8.50 except as noted. ^b Cathodic peak potential, E_{pc} , and peak width parameter, $E_{pc} - E_{p/2}$ (in parentheses), for the initial reduction step of the *trans*-Cr^{III}N₂O₄ complexes. ^c Formal potential of the chemically reversible couple observed following one-electron reduction of the *trans*-Cr^{III}N₂O₄ complexes (see Figure 1d and text). ^d pH 6.1. ^e pH 5.0. ^f From ref 36; $\mu = 0.1 \text{ M}$ (LiClO_4), pH 4–6.

better approximations, especially for cases with large homogeneous rate constants (spline collocation)²⁰ and nonstationary diffusion layers (expanding simulation space).²¹ The program was implemented on the CONVEX C220 of the Zentrum für Datenverarbeitung der Universität Tübingen, Germany, and was run under the UNIX operating system. The following mechanistic models were used to simulate cyclic voltammetric responses of chromium amino carboxylate complexes: E_{qr} (quasi-reversible electron transfer),²² EC (reversible electron transfer with irreversible follow-up reaction),²³ and $E_{qr}C$ (quasi-reversible electron transfer with irreversible follow-up reaction).²⁴ Simulations of the full square scheme and in some cases of the mechanisms discussed above also were performed with DigiSim (Bioanalytical Systems, Inc., West Lafayette, IN). DigiSim relies on the FIFD algorithm²⁵ and was used with the default settings of the simulation parameters. The temperature was set to 293 K.

Evaluation of Cyclic Voltammograms. Cyclic voltammograms were analyzed by the multiparametric fitting technique described earlier^{22–24} for E_{qr} , EC, and $E_{qr}C$ mechanisms using the programs FEATURE and ESTIMAT. FEATURE is used to generate response functions by polynomial regression of simulated data for various features of a cyclic voltammogram [e.g., peak potential (E_p), half-peak potential ($E_{p/2}$), and peak current function (χ_p)]. ESTIMAT compares the resulting response surfaces to experimental data recorded as a function of scan rate and obtains a best fit between experimental and simulated results by nonlinear optimization (Levenberg–Marquardt algorithm) of the parameters of the chemical system under investigation [e.g., the homogeneous rate constants (k), heterogeneous electron transfer rate constants ($k_{s,h}$), and redox potentials (E°)]. These terms are called the “system parameters”.

Results

Structural and Spectroscopic Properties. Coordination environments of the chromium complexes investigated in this

work are illustrated in Chart 2. With the exception of *trans*-N₂O₃O', these descriptions are taken from X-ray crystal structures of isolated compounds, and it is assumed (except as noted) that the geometry in solution is the same as that found in the solid state. The *cis*-N₂O₄ (A) structure occurs in $\text{K}[\text{Cr}(\text{IDA})_2] \cdot 3\text{H}_2\text{O}$,²⁶ where the iminodiacetate ligands bind the metal in a facial tridentate manner with the nitrogen donors coordinated *cis* to one another. However, in analogous *N*-alkyliminodiacetate (RIDA) complexes, the nitrogen atoms occupy *trans* positions presumably to avoid steric interaction between alkyl substituents. Thus, the *trans*-N₂O₄ geometry is found in X-ray crystal structures of the *N*-isopropyl²⁷ and *N*-*tert*-butyl²⁸ derivatives of the bis(iminodiacetate) complex; it almost certainly occurs in the structure of the *N*-methyl derivative as well. Complexes with hexadentate amino carboxylate ligands exhibit the *cis*-N₂O₄ (B) environment if the ligand framework provides sufficient strain relief for binding of the in-plane carboxylates. Examples are found in the structures of $\text{Na}[\text{Cr}(1,3\text{-PDTA})] \cdot \text{H}_2\text{O}$ ²⁹ and $\text{Li}[\text{Cr}(\text{EDDDA})] \cdot 5\text{H}_2\text{O}$.³⁰ The *cis*-N₂O₃O' structure occurs in complexes such as $\text{Cr}(\text{MED3A})(\text{H}_2\text{O})$ which have a rigorously pentadentate ligand. However, if a hexadentate ligand lacks the necessary flexibility, one of the in-plane carboxylates may become detached, producing a pentadentate ligand and allowing a water molecule to become coordinated to the metal. This *cis*-N₂O₃O' structure, which is found in the $\text{Cr}(\text{HEDTA})(\text{H}_2\text{O})$ complex isolated at low pH,³¹ is presumed to occur in the solution structures of the EDTA and CyDTA complexes throughout our investigations.³²

Chromium(III) complexes in the above coordination environments exhibit characteristic electronic spectra and voltammetric responses. Spectroscopic data are collected in Table 1. For the *trans*-N₂O₄ complexes, absorptions arising from the

(17) Villadsen, J.; Michelsen, M. L. *Solution of Differential Equation Models by Polynomial Approximation*; Prentice-Hall: Englewood Cliffs, NJ, 1978.

(18) Whiting, L. F.; Carr, P. N. *J. Electroanal. Chem. Interfacial Electrochem.* **1977**, *81*, 1.

(19) Pons, S. In *Electroanalytical Chemistry*; Bard, A. J., Ed.; Marcel Dekker: New York, 1984; Vol. 13, pp 115–190.

(20) Hertil, P.; Speiser, B. *J. Electroanal. Chem. Interfacial Electrochem.* **1987**, *217*, 225.

(21) Urban, P.; Speiser, B. *J. Electroanal. Chem. Interfacial Electrochem.* **1988**, *241*, 17.

(22) Scharbert, B.; Speiser, B. *J. Chemom.* **1988**, *3*, 61.

(23) Speiser, B. *Anal. Chem.* **1985**, *57*, 1390.

(24) Speiser, B.; Hecht, M., unpublished work.

(25) (a) Rudolph, M. *J. Electroanal. Chem. Interfacial Electrochem.* **1991**, *314*, 13. (b) Rudolph, M. *J. Electroanal. Chem. Interfacial Electrochem.* **1992**, *328*, 85. (c) Rudolph, M.; Reddy, D. P.; Feldberg, S. W. *Anal. Chem.* **1994**, *66*, 589A.

(26) Mootz, D.; Wunderlich, H. *Acta Crystallogr.* **1980**, *B36*, 445.

(27) Mootz, D.; Wunderlich, H. *Acta Crystallogr.* **1980**, *B36*, 721.

(28) Mootz, D.; Wunderlich, H. *Acta Crystallogr.* **1980**, *B36*, 1189.

(29) Herak, R.; Srdanov, G.; Djuran, M. I.; Radanovic, D. J.; Bruvo, M. *Inorg. Chim. Acta* **1982**, *83*, 55.

(30) Helm, F. T.; Watson, W. H.; Radanovic, D. J.; Douglas, B. E. *Inorg. Chem.* **1977**, *16*, 2351.

(31) Gerdorf, L. E.; Baenziger, N. A.; Goff, H. M. *Inorg. Chem.* **1981**, *20*, 1606.

(32) The solution structure of Cr(III)–EDTA and of related complexes at neutral pH is a controversial topic. Alternatives to the *cis*-N₂O₃O' geometry include a six-coordinate *cis*-N₂O₄ (B) structure in which all of the ligand's donor atoms are coordinated to the metal, a seven-coordinate $\text{Cr}(\text{EDTA})(\text{H}_2\text{O})^-$ structure in which one molecule of water is added to this set, and a labile quinqueximate–sexidentate equilibrium between *cis*-N₂O₃O' and *cis*-N₂O₄(B) geometries.^{33,34}

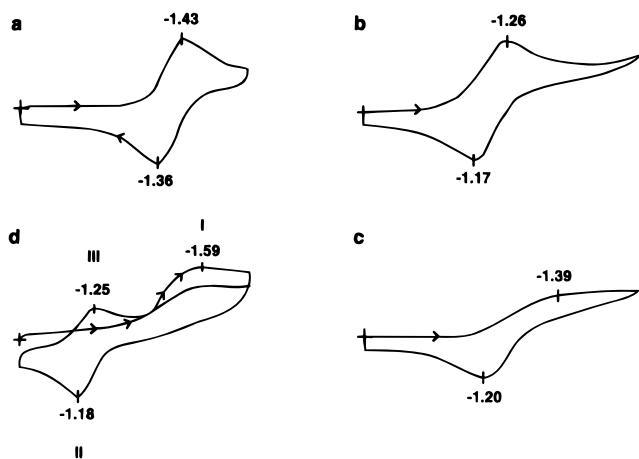
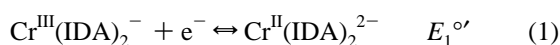


Figure 1. Cyclic voltammetric reductions: (a) 1 mM $\text{Cr}(\text{IDA})_2^-$, 0.1 M IDA, pH 8.5, $\mu = 1.0$ (Na_2SO_4), $\nu = 5.12 \text{ V s}^{-1}$; (b) 2 mM $\text{Cr}(\text{CyDTA})(\text{H}_2\text{O})^-$, 0.1 M CyDTA, 0.5 M NaClO_4 , pH 8.4, $\nu = 0.2 \text{ V s}^{-1}$; (c) as in (b) except pH 10.6, $\nu = 0.5 \text{ V s}^{-1}$; (d) 1 mM $\text{Cr}(\text{MIDA})_2^-$, 0.1 M MIDA, pH 8.5, $\mu = 1.0$ (Na_2SO_4), $\nu = 5.12 \text{ V s}^{-1}$.

$^4\text{A}_{2g} \rightarrow ^4\text{T}_{2g}$ and $^4\text{A}_{2g} \rightarrow ^4\text{T}_{1g}$ transitions in approximate O_h symmetry³⁷ occur at ca. 500 and 360 nm and have molar absorptivities of ca. 40 and $28 \text{ M}^{-1} \text{ cm}^{-1}$, respectively. In the *cis*- N_2O_4 environment, these absorptions shift to lower energies and increase in intensity. When water replaces a carboxylate group to produce the *cis*- $\text{N}_2\text{O}_3\text{O}'$ donor atom set, the lower energy absorption shifts to still longer wavelengths and experiences a further increase in intensity.

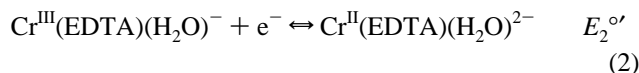
Electrochemical Properties. Figure 1 illustrates the general electrochemical behavior of the Cr(III) amino carboxylate complexes. The cyclic voltammogram in Figure 1a is representative of the IDA, 1,3-PDTA, and EDDDA complexes which have a *cis*- N_2O_4 (A) or *cis*- N_2O_4 (B) environment. Each compound undergoes a chemically and electrochemically reversible one-electron reduction at a formal potential, $E_1^{\circ'}$, between -1.35 and -1.43 V (Table 1). Supporting Table S1 contains data illustrating the electrochemical behavior of the bis(iminodiacetate) complex to which the following electrode reaction is assigned:



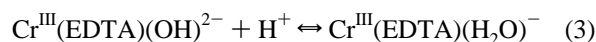
The results in Table S1 show that the cathodic peak potential, E_{pc} , and cathodic peak current function, $i_{\text{pc}}/\nu^{1/2}$, are independent of scan rate, ν , and that the peak potential separation, ΔE_{p} , is only slightly larger than 58 mV. A lower limit of $(k_{\text{s,h}})_1 \geq 0.2 \text{ cm s}^{-1}$ is estimated for the standard heterogeneous electron transfer rate constant of reaction 1 by the method of Nicholson.³⁸

The cyclic voltammogram in Figure 1b depicts the electrochemical behavior of the CyDTA complex at pH 8.4 and is characteristic of compounds containing the *cis*- $\text{N}_2\text{O}_3\text{O}'$ coordination environment at approximately neutral pH values. Data for reduction of the Cr(III)-EDTA complex under similar conditions are presented in supporting Table S2. The response

is characterized by a small negative shift in E_{pc} , a small decrease in $i_{\text{pc}}/\nu^{1/2}$, and a small increase in ΔE_{p} above 58 mV with increasing sweep rate. A value of $(k_{\text{s,h}})_2 \geq 0.08 \text{ cm s}^{-1}$ is estimated from the sweep rate dependence of ΔE_{p} . This result is consistent with the quasi-reversible one-electron reduction of $\text{Cr}(\text{EDTA})(\text{H}_2\text{O})^-$ reported independently by Bard⁵ and by Tanaka.³⁹ In neutral solution reduction of these compounds is described by reaction 2 and occurs at a formal potential of $E_2^{\circ'} = -1.19$ to -1.24 V (Table 1).



An additional characteristic of the *cis*- $\text{N}_2\text{O}_3\text{O}'$ complexes is the voltammetric behavior at high pH that is illustrated in Figure 1c. The coordinated water molecule is deprotonated under these conditions,⁴⁰ and the resulting hydroxo complex is reduced less easily than the starting material. It is proposed⁴¹ that reduction of the Cr(III) complex proceeds through the protonation equilibrium shown in eq 3 prior to reaction 2. The plateau-



shaped i - E response in Figure 1c signifies kinetic limitation of the faradaic current and is characteristic of this sequence of events.⁴²

Figure 1d depicts the voltammetric behavior of Cr(III)-MIDA, which typifies compounds that have a *trans*- N_2O_4 coordination environment. The initial step in the reduction of $\text{Cr}(\text{MIDA})_2^-$ (peak I) is a broad cathodic response for which the peak potential shifts from ca. -1.4 V at small scan rates to ca. -1.6 V at large ones. The cathodic peak current is proportional to the square root of scan rate, but the peak width parameter ($E_{\text{pc}} - E_{\text{p}2}$) is larger than the 57 mV value that is characteristic of a reversible one-electron transfer.⁴³ No anodic peak associated with peak I is detected on scan reversal. These observations indicate that the kinetics of electrochemical reduction of $\text{Cr}(\text{MIDA})_2^-$ are sluggish and that the electron transfer is followed by a rapid chemical reaction. Data supporting these conclusions are presented in Table S3 in the Supporting Information.

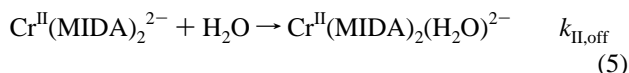
If the voltammetric scan in Figure 1d is continued first in the positive and then in the negative direction following $\text{Cr}(\text{MIDA})_2^-$ reduction, a chemically reversible couple characterized by an anodic peak at -1.18 V (peak II) and a cathodic one at -1.25 V (peak III) is observed on the second and third half-cycles, respectively. The formal potential $E_2^{\circ'} = -1.21 \text{ V}$ of the newly generated couple lies within the range of values observed for $\text{Cr}^{\text{III/II}}$ couples that contain a donor atom set consisting of one aquo, two amine, and three carboxylate ligands (Table 1, Figure 1b). On the basis of this evidence, we conclude that the coordination environment of $\text{Cr}(\text{MIDA})_2^-$ changes from N_2O_4 to $\text{N}_2\text{O}_3\text{O}'$ following its electrochemical reduction.

The electrochemical behavior illustrated in Figure 1d can be interpreted in terms of an electrochemical square scheme⁴⁴ as shown in Figure 2. Starting with $\text{Cr}(\text{MIDA})_2^-$, the first two steps in the mechanism (top and right) consist of the one-electron reduction of *trans*- $\text{Cr}^{\text{III}}\text{N}_2\text{O}_4$ (reaction 4) followed by cleavage of a Cr-carboxylate bond and addition of water to produce

- (33) (a) Thorneley, R. N. F.; Sykes, A. G.; Gans, P. *J. Chem. Soc. A* **1971**, 1494. (b) Wheeler, W. D.; Legg, J. I. *Inorg. Chem.* **1984**, *23*, 3798. (c) Ogino, H.; Shimura, M. *Adv. Inorg. Bioinorg. Mech.* **1986**, *4*, 107. (d) Kanamori, K.; Kawai, K. *Inorg. Chem.* **1986**, *25*, 3711. (e) Pletcher, D.; White, J. C. P. *Electrochim. Acta* **1992**, *37*, 575. (f) Yoshitani, K. *Bull. Chem. Soc. Jpn.* **1994**, *67*, 2115.
- (34) Beswick, C. L.; Shalders, R. D.; Swaddle, T. W. *Inorg. Chem.* **1996**, *35*, 991.
- (35) Ogino, H.; Watanabe, T.; Tanaka, N. *Inorg. Chem.* **1975**, *14*, 2093.
- (36) Ogino, H.; Nagata, T.; Ogino, K. *Inorg. Chem.* **1989**, *28*, 3656.
- (37) Perumareddi, J. R. *Coord. Chem. Rev.* **1969**, *4*, 73.
- (38) Nicholson, R. S. *Anal. Chem.* **1965**, *37*, 1351.

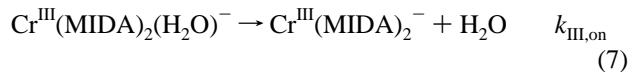
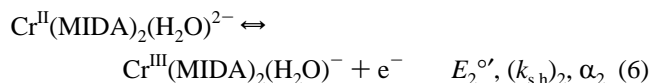
- (39) Yamada, A.; Tanaka, N. *Bull. Chem. Soc. Jpn.* **1969**, *42*, 1600.
- (40) The pK_a of the coordinated water in $\text{Cr}(\text{EDTA})(\text{H}_2\text{O})^-$ is 7.4.³⁵
- (41) Tang, T.-W.; Anson, F. C. *J. Electroanal. Chem. Interfacial Electrochem.* **1984**, *177*, 183.
- (42) (a) Nicholson, R. S.; Shain, I. *Anal. Chem.* **1964**, *36*, 706. (b) Saveant, J.-M.; Vianello, E. *Electrochim. Acta* **1963**, *8*, 905.
- (43) Bard, A. J.; Faulkner, L. R. *Electrochemical Methods: Fundamentals and Applications*; Wiley: New York, 1980; pp 215–227.

a *trans*-Cr^{II}N₂O₃O' species (reaction 5). The rate constant



designated $k_{\text{II,off}}$ corresponds to displacement of a bound carboxylate group in the Cr(II) oxidation state. This segment of the mechanism possesses elements of both chemical and electrochemical irreversibility. The failure to observe an anodic peak associated with peak I was noted earlier. At sweep rates above 1 V s⁻¹, the cathodic peak width parameter and the sweep rate dependence of the cathodic peak potential for Cr(MIDA)₂⁻ reduction are independent of ν and exhibit values of ($E_{\text{pc}} - E_{\text{p}2}$) = 0.155 and ($\Delta E_{\text{pc}}/\Delta \log \nu$) = 0.113 V, respectively. This behavior is consistent with irreversible electron transfer.⁴³ At sweep rates below 1 V s⁻¹, the magnitudes of $E_{\text{pc}} - E_{\text{p}2}$ and $\Delta E_{\text{pc}}/\Delta \log \nu$ are smaller and sweep rate dependent yet are still larger than values that are characteristic of a reversible electron transfer. Under these conditions, the overall electrochemical response is influenced simultaneously by the heterogeneous kinetics of reaction 4 and the chemical kinetics of reaction 5 and is classified as an E_{qr}C mechanism.⁴⁵

The second half of the square scheme (Figure 2, bottom and left) consists of electrochemical reoxidation of the *trans*-Cr^{II}N₂O₃O' center (reaction 6) followed by reattachment of the displaced carboxylate arm and loss of water to produce the original *trans*-Cr^{III}N₂O₄ reactant (reaction 7). The rate constant $k_{\text{III,on}}$ designates reattachment of the carboxylate group in the Cr(III) oxidation state. At scan rates above ca. 5 V s⁻¹, peaks



II and III are approximately equal in height and $\Delta E_p \approx 70$ mV (as shown in Figure 1d).

The influence of the chemical follow-up reaction described by eq 7 becomes apparent if we look at cyclic voltammograms which examine the oxidation of Cr(II) at slower sweep rates. The chromium(II) complex could not be isolated as a solid due to its high oxidizability. Consequently, Cr^{II}(MIDA)₂(H₂O)²⁻ was generated from Cr^{III}(MIDA)₂⁻ *in situ* by holding the working electrode potential at $E = -1.6$ V for a time (15–60 s) sufficient to produce a steady-state concentration of the structurally rearranged Cr^{II} product in the diffusion layer. Then, the potential was swept in the positive direction at different values of ν and reversed at ca. -0.95 V. The resulting cyclic voltammograms are shown in Figure 3, where oxidation of

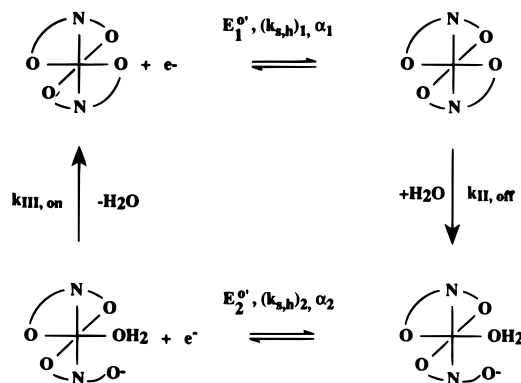


Figure 2. Proposed mechanism for electrochemical reduction of Cr(RIDA)₂⁻ complexes.

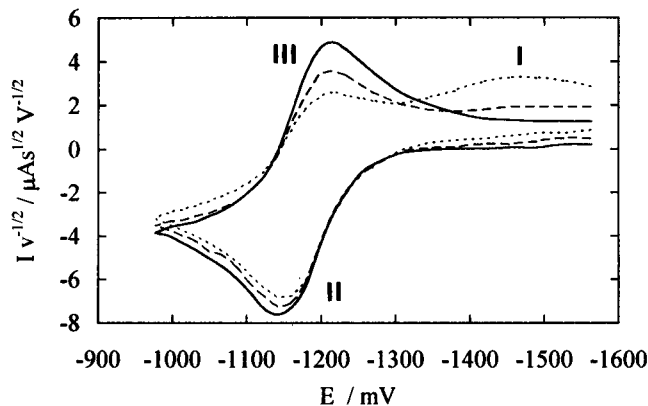


Figure 3. Scan rate normalized cyclic voltammograms for electrooxidation of Cr^{II}(MIDA)₂(H₂O)²⁻ generated *in situ* by controlled-potential reduction of Cr^{III}(MIDA)₂⁻ at -1.6 V. Scan rates (V s⁻¹): 20.5 (—); 2.0 (---); 0.5 (···).

Cr^{II}(MIDA)₂(H₂O)²⁻ to Cr^{III}(MIDA)₂(H₂O)⁻ occurs according to eq 6 (peak II) and the corresponding re-reduction occurs by the reverse of this reaction (peak III). At scan rates below 20 V s⁻¹ the current of peak III decreases relative to that of peak II, which reflects conversion of the Cr^{III} complexes according to eq 7. The appearance of a broad response at ca. -1.5 V (peak I) at these slower scan rates is attributed to reduction of *trans*-Cr^{III}(MIDA)₂⁻ via eq 4 and signals completion of the square scheme. Complexes with EIDA, *n*-PIDA, and *n*-BIDA ligands exhibit similar behavior.

Determination of Electrode Reaction Parameters. Quantitative evaluation of the parameters in the electrochemical square scheme was accomplished for the MIDA and EIDA complexes by means of the multiparametric fitting procedure described in the Experimental Section. To carry out this analysis, the reaction mechanism in Figure 2 was divided into two parts according to the discussion above: (i) reduction of Cr^{III}(RIDA)₂⁻ and subsequent attack of water leading to displacement of one carboxylate donor (E_{qr}C mechanism, eqs 4 and 5) and (ii) reoxidation of Cr^{II}(RIDA)₂(H₂O)²⁻ and reattachment of the pendant carboxylate group accompanied by loss of H₂O (EC mechanism, eqs 6 and 7).

The E_{qr}C mechanism reduction is described by the system parameters $E_1^{o'}$, $(k_{s,h})_1$, α_1 , and $k_{\text{II,off}}$. The data in supporting Table S3 show that $E_{\text{pc}} - E_{\text{p}2}$ and $\Delta E_{\text{pc}}/\Delta \log \nu$ for Cr(MIDA)₂⁻ reduction are independent of scan rate at $\nu \geq 1$ V s⁻¹. The same is true for Cr(EIDA)₂⁻ reduction. Under these conditions, the transfer coefficient α_1 is defined by⁴³ $\alpha_1 = 0.0477/(E_{\text{pc}} - E_{\text{p}2})$ and $\alpha_1 = 0.0296/(\Delta E_{\text{pc}}/\Delta \log \nu)$ for a one-electron transfer. From data for the MIDA and EIDA complexes, $\alpha_1 \approx 0.30$. This value was used to model reactions 4 and 5 as an E_{qr}C mechanism

- (44) (a) Bond, A. M.; Oldham, K. B. *J. Phys. Chem.* **1983**, *87*, 2492. (b) Vallat, A.; Person, M.; Roullier, L.; Laviron, E. *Inorg. Chem.* **1987**, *26*, 332. (c) Lerke, S. A.; Evans, D. H.; Feldberg, S. E. *J. Electroanal. Chem. Interfacial Electrochem.* **1990**, *296*, 299. (d) Evans, D. H. *Chem. Rev.* **1990**, *90*, 139. (e) Araki, K.; Shu, C. F.; Anson, F. C. *Inorg. Chem.* **1991**, *30*, 3043. (f) Balducci, G.; Costa, G. *J. Electroanal. Chem. Interfacial Electrochem.* **1993**, *348*, 355. (g) Robandt, P. V.; Schroeder, R. R.; Rorabacher, D. B. *Inorg. Chem.* **1993**, *32*, 3957. (h) Richards, T. C.; Geiger, W. E. *J. Am. Chem. Soc.* **1994**, *116*, 2028. (45) (a) Evans, D. H. *J. Phys. Chem.* **1972**, *76*, 1160. (b) Nadjo, L.; Saveant, J. M. *J. Electroanal. Chem. Interfacial Electrochem.* **1973**, *48*, 113. (c) Klingler, R. J.; Kochi, J. K. *J. Phys. Chem.* **1981**, *85*, 1731. (d) Huang, Q.; Gosser, D. K., Jr. *Talanta* **1992**, *39*, 1155. (e) Kumar, V. T.; Birke, R. L. *Anal. Chem.* **1993**, *65*, 2428.

Table 2. System Parameters for Cr^{III} Redox Couples with *N*-Alkyliminodiacetate Ligands^{a,b}

ligand	redn of Cr ^{III} -N ₂ O ₄ centers				oxidn of Cr ^{II} -N ₂ O ₃ O' centers			
	$E_1^{o'}$, V	$(k_{s,h})_1$, cm s ⁻¹	α_1	$k_{II,off}$, s ⁻¹	$E_2^{o'}$, V	$(k_{s,h})_2$, cm s ⁻¹	α_2	$k_{III,on}$, s ⁻¹
MIDA	-1.402 ± 0.003	(2.0 ± 0.2) × 10 ⁻³	0.30 ± 0.01	35 ± 6	-1.209 ± 0.005	0.20 ± 0.01	0.76 ± 0.05	1.3 ± 0.2
EIDA	-1.386 ± 0.014	(1.0 ± 0.1) × 10 ⁻²	0.30 ± 0.02	730 ± 340	-1.173 ± 0.022	≥ 0.1		220 ± 20

^a 1 mM complex, 0.1 M ligand, $\mu = 1.0$ M (Na₂SO₄), pH 8.50. ^b Error limits for the system parameters determined by multiparameter fitting are calculated from approximate 95% confidence contours: Draper, N. R.; Smith, H. *Applied Regression Analysis*; Wiley: New York, 1966; p 292 ff.

under cyclic voltammetric conditions at $v < 1$ V s⁻¹, where the experimental response is determined by the kinetics of both electron transfer and the chemical follow-up reaction. Simulated results for the cathodic peak current function ($\pi^{1/2}\chi_{pc}$), the half-peak potential referred to $E_1^{o'}$ ($E_{p/2} - E_1^{o'}$), and the half-peak width ($E_{pc} - E_{p/2}$) as a function of $\psi = (k_{s,h})_1/(aD)^{1/2}$ and $\kappa = k_{II,off}/a$ ($a = Fv/RT$) were described by polynomials.²⁴ A fit between these polynomials and experimental values of i_{pc} , $E_{p/2}$, and $E_{pc} - E_{p/2}$ (Table S3) was obtained by adjusting $(k_{s,h})_1$ and $k_{II,off}$ such that the residual sum of squares S_R^2 between simulated and experimental results reached a minimum. Using as an example the $E_{p/2}$ data for Cr(MIDA)₂²⁻ reduction, supporting Figure S1 shows that a plot of log S_R^2 versus log $k_{II,off}$ and log $(k_{s,h})_1$ exhibits an unambiguous global minimum at $k_{II,off} = 35 \pm 6$ s⁻¹ and $(k_{s,h})_1 = (2.0 \pm 0.1) \times 10^{-3}$ cm s⁻¹. Furthermore, from this procedure $E_1^{o'} = -1.402 \pm 0.003$ V was determined. System parameters for the ethyl-substituted derivative were determined in a similar way. Results for the MIDA and EIDA complexes are summarized in Table 2.

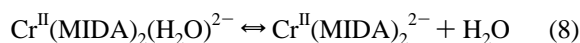
The reoxidation reactions of Cr(MIDA)₂(H₂O)²⁻ and Cr(EIDA)₂(H₂O)²⁻ are Nernstian electrode processes at slow scan rates; thus, reactions 6 and 7 were modeled as a reversible electron transfer followed by an irreversible chemical reaction with $E_2^{o'}$ and $k_{III,on}$ as the system parameters. These quantities were determined from experiments in which the Cr^{II} species was generated *in situ* by pre-electrolysis. Representative data for Cr(MIDA)₂(H₂O)²⁻ oxidation are presented in supporting Table S4. Peak potential (E_p^{II}) and peak current ratio (i_{pIII}/i_{pII}) data at scan rates between 0.4 and 20.5 V s⁻¹ from two independent experiments were compared to simulated values.²³ For the MIDA complex, global minima were found for log S_R^2 which represent the optimum fit between experimental and simulated data. Results for $E_2^{o'}$ and $k_{III,on}$ are given in Table 2. In comparison with that for the MIDA complex, the follow-up reaction (eq 7) is much faster in the case of Cr(EIDA)₂(H₂O)²⁻ oxidation. Consequently, for this complex $k_{III,on}$ was determined from i_{pIII}/i_{pII} data at scan rates above 50 V s⁻¹, where the reverse peak can be observed, while $E_2^{o'}$ was obtained from E_p^{II} data at scan rates below 50 V s⁻¹, where the electron transfer is reversible.

At fast scan rates, the electrochemical oxidation of Cr(MIDA)₂(H₂O)²⁻ (eq 6) becomes quasi-reversible. At the same time, the effect of the follow-up chemical reaction (eq 7) disappears. Data obtained at $68 \leq v \leq 204$ V s⁻¹ were analyzed by the multiparametric fitting procedure assuming eq 6 to be a quasi-reversible electron transfer (E_{qr} model),²³ and values of $(k_{s,h})_2$ and α_2 were determined for this oxidation. The results also are given in Table 2. This analysis was not possible for the EIDA complex because even at the highest attainable scan rate of 204 V s⁻¹ the follow-up reaction could not be neglected. A lower limit of $(k_{s,h})_2 \geq 0.1$ cm s⁻¹ is estimated from the peak potential separation at this scan rate for this redox couple.

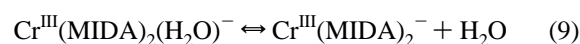
Results for the *n*-PIDA and *n*-BIDA complexes were not analyzed quantitatively. However, the rate constants of heterogeneous electron transfer ($k_{s,h}$) and chemical reaction ($k_{II,off}$ and $k_{III,on}$) for these species were observed to be equal to or greater than those of the EIDA complex.

Further Mechanistic Aspects. As a means of verifying the assertion that a square scheme is operative in the reduction of the *trans*-Cr(RIDA)₂⁻ complexes, a number of simulations were carried out with DigiSim,²⁵ which became commercially available while this work was in progress. DigiSim results are a useful qualitative test of the validity of mechanism assignment. This software also provides a convenient means of assessing the importance of the homogeneous redox cross-reaction^{44h} in the electrochemical square scheme.

Because DigiSim considers homogeneous reactions as equilibrium processes, it is necessary to re-express eqs 5 and 7 as follows:



$$K_{\text{II}} = k_{\text{II,on}}/k_{\text{II,off}}$$



$$K_{\text{III}} = k_{\text{III,on}}/k_{\text{III,off}}$$

The system is bound by the relation $K_{\text{III}}/K_{\text{II}} = \exp[(F/RT)(E_2^{o'} - E_1^{o'})]$,⁴⁶ which for the MIDA ligand equals 1.84×10^3 . One more parameter is needed to describe the square scheme completely; for this we choose $K_{\text{III}} = [\text{Cr}^{\text{III}}(\text{MIDA})_2^{-}]/[\text{Cr}^{\text{III}}(\text{MIDA})_2(\text{H}_2\text{O})^{-}]$. Figure 4 shows simulations with K_{III} set equal to 10, 10² and 10³ for Cr(MIDA)₂⁻ reduction via reactions 4, 6, 8, and 9 at $v = 5.12$ V s⁻¹ employing values for formal potentials, transfer coefficients, electrochemical rate constants and homogeneous rate constants given in Table 2. The simulated curve for $K_{\text{III}} = 10^2$ closely matches the experimental trace in Figure 1d. This agreement supports the conclusion that a square scheme is operative in the reduction of Cr(MIDA)₂⁻ and that $K_{\text{III}} = 100$ and hence $K_{\text{II}} = 5.4 \times 10^{-2}$ are valid approximate values for the equilibrium constants of reactions 8 and 9. Figure 4 also shows that when $K_{\text{III}} = 10$, a small cathodic peak corresponding to Cr^{III}(MIDA)₂(H₂O)⁻ reduction is observed at ca. -1.2 V on the initial negative scan and that, when $K_{\text{III}} = 1000$, a shoulder corresponding to Cr^{II}(MIDA)₂²⁻ oxidation is observed at ca. -1.3 V on the positive scan. Neither feature is observed experimentally, which is consistent with the assumption that the equilibrium constant of reaction 9 is in the range $10 < K_{\text{III}} < 1000$.

As an additional test of mechanism assignment, simulated and experimental curves were compared at several different scan rate values for Cr(MIDA)₂⁻ reduction. Supporting Figure S2 shows the results of such comparisons for two sets of conditions: $K_{\text{III}} = 100$, $v = 0.05$ V s⁻¹ and $K_{\text{III}} = 100$, 5.12 V s⁻¹. Good qualitative agreement is observed between simulated and experimental curves, which provides additional support for the existence of the square scheme and the numerical values of the system parameters in Table 2.

Digital simulation also enabled us to investigate the possible involvement of the redox cross-reaction

(46) Luo, W.; Feldberg, S. W.; Rudolph, M. *J. Electroanal. Chem. Interfacial Electrochem.* **1994**, 368, 109.

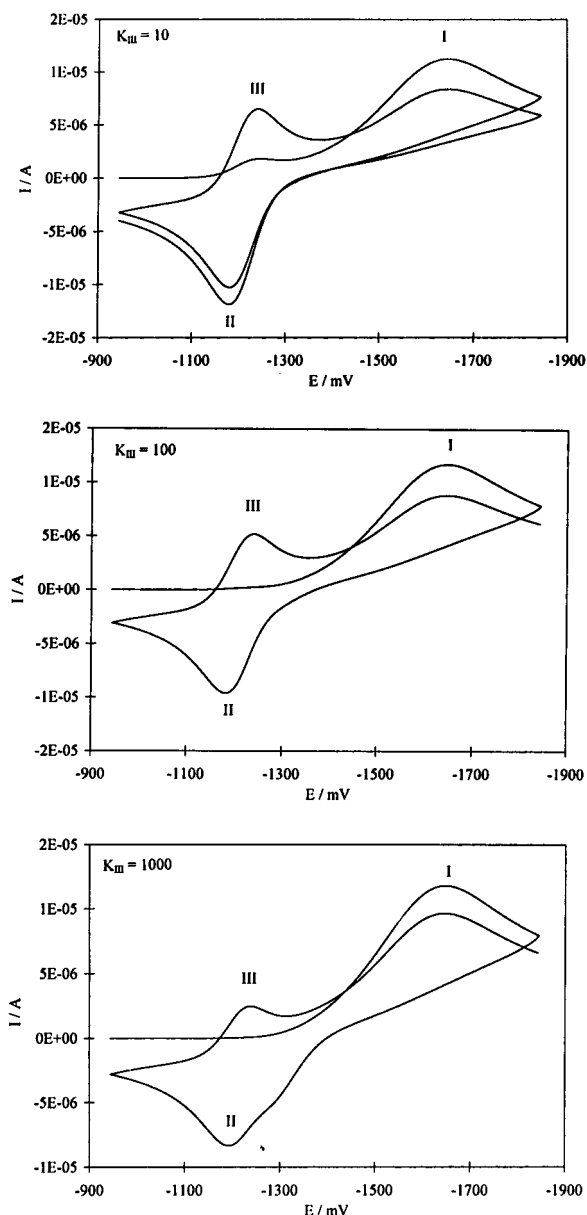
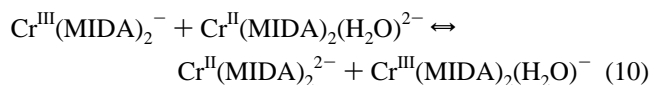


Figure 4. Cyclic voltammograms simulated by DigiSim with K_{III} set equal to 10, 100, and 1000 for reduction of 1 mM $\text{Cr}(\text{MIDA})_2^-$ according to reactions 4, 6, 8, and 9 at 5.12 V s^{-1} employing the system parameters in Table 2, an electrode area of 0.015 cm^2 , and a diffusion coefficient of $4.6 \times 10^{-6} \text{ cm}^2 \text{ s}^{-1}$ for all species.



$$K_{\text{cross}} = k_{\text{f,cross}}/k_{\text{b,cross}}$$

in the electrochemical square scheme. Although reaction 10 is thermodynamically unfavorable $\{K_{\text{cross}} = \exp[(F/RT)(E_1^{o'} - E_2^{o'})] = 5.4 \times 10^{-4}\}$, its presence can alter the voltammetric response even when reactants are present under equilibrium conditions. One experimental consequence^{44h} of the cross-reaction is an enhancement in cathodic current at the potential of the more easily reduced substance (peak III in this case) relative to the value at $k_{\text{f,cross}} = 0$. Digital simulation of the Cr(III)–MIDA square scheme including reaction 10 was carried out at scan rates of 0.05 and 5.12 V s^{-1} using experimental conditions and system parameters given earlier. The simulated voltammetric response was not influenced by the presence of the cross-reaction for values of $k_{\text{f,cross}} \leq 1 \times 10^5 \text{ M}^{-1} \text{ s}^{-1}$. At

larger values of this rate constant, enhanced reversibility of the $\text{Cr}(\text{MIDA})_2^{-2-}$ couple is observed [presumably by electron transfer mediation by $\text{Cr}(\text{MIDA})_2(\text{H}_2\text{O})^{-2-}$] as evidenced by a narrowing of peak I and the appearance of an anodic shoulder on the negative side of peak II in the simulated voltammograms. These features are not observed experimentally. Consequently, we conclude that $k_{\text{f,cross}} < 1 \times 10^5 \text{ M}^{-1} \text{ s}^{-1}$ and that the cross-reaction is not an important element in the square scheme.

Discussion

Correlation of Chromium(III) Coordination Environments with Spectroscopic and Electrochemical Properties.

The chromium(III) coordination environments illustrated in Chart 2 can be distinguished on the basis of their spectroscopic and electrochemical properties. The distinction between *cis* and *trans* $\text{Cr}^{\text{III}}\text{-N}_2\text{O}_4$ centers (Table 1) is consistent with earlier spectroscopic assignments^{10,11,13,37} based on Cr(III) $d \rightarrow d$ transition energies and intensities. Larger molar absorptivities are observed for the *cis*- N_2O_4 environment, consistent with its lower symmetry. Replacement of one carboxylate donor by H_2O leads to a further reduction in symmetry and a small increase in intensity of the lower energy band.

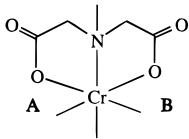
The Cr(III/II) redox potential provides a second means of characterizing the amino carboxylate coordination environment. *Cis*- N_2O_4 and *trans*- N_2O_4 complexes, which contain two amine and four carboxylate donors, undergo reduction at $E_1^{o'} = -1.35$ to -1.46 V . *Cis*- $\text{N}_2\text{O}_3\text{O}'$ and *trans*- $\text{N}_2\text{O}_3\text{O}'$ complexes are reduced at $E_2^{o'} = -1.19$ to -1.24 V . Thus, the number and type of donor atoms are the primary determinant of the Cr(III/II) potential.⁴⁷ The ranges of values observed for $E_1^{o'}$ and $E_2^{o'}$ coincide with the results of Ogino et al.,³⁶ who reported Cr^{III/II} potentials of -1.36 ± 0.05 and $-1.22 \pm 0.04 \text{ V}$ for hexadentate and (aquo) pentadentate amino carboxylate complexes, respectively. A difference in formal potentials is anticipated on the basis of the differing electron donor strengths of aquo and carboxylate ligands. A recent parametrization of metal complex redox potentials⁴⁸ predicts a shift of ca. $+0.2 \text{ V}$ upon replacement of $-\text{CO}_2^-$ by H_2O . The observed difference between $E_1^{o'}$ and $E_2^{o'}$ is consistent with this estimate.

Cis- and *trans*- N_2O_4 complexes, however, do exhibit differences in the rate and mechanism of Cr(III) reduction as illustrated by the cyclic voltammograms in Figure 1a,d. Reduction of *cis*- N_2O_4 complexes is electrochemically reversible and uncomplicated by chemical follow-up reactions. Electrochemical reduction of *trans*- N_2O_4 complexes initiates the sequence of chemical and electrochemical events described in Figure 2. The mechanisms of these reactions and reasons for the difference in behavior exhibited by complexes with *cis* versus *trans* nitrogen donors are discussed in the following section.

Rates and Mechanisms of the Cr(III/II) Electrode Reactions. One difference in electrochemical behavior between the *trans*- $\text{Cr}(\text{RIDA})_2^-$ complexes and their *cis*- N_2O_4 analogs is the magnitude of the heterogeneous rate constant of the Cr^{III/II} electrode reaction (Table 2). We measure $(k_{\text{s,h}})_1 \geq 0.2 \text{ cm s}^{-1}$ for $\text{Cr}(\text{IDA})_2^{-2-}$, $(k_{\text{s,h}})_1 = 2 \times 10^{-3} \text{ cm s}^{-1}$ for $\text{Cr}(\text{MIDA})_2^{-2-}$, and $(k_{\text{s,h}})_1 = 1 \times 10^{-2} \text{ cm s}^{-1}$ for $\text{Cr}(\text{EIDA})_2^{-2-}$. Since the size and electrostatic charge of the $\text{Cr}(\text{IDA})_2^{-2-}$ and $\text{Cr}(\text{RIDA})_2^-$ complexes are nearly identical, variations in their heterogeneous rate constants must derive predominantly from inner-shell contributions to electrochemical activations. Differences in double-layer effects will be small because the compounds are reduced at nearly the same potential. By use of the Marcus

(47) *Cis* and *trans* isomers of coordination complexes with identical donor atom sets generally do not have very different formal potentials.⁴⁸

(48) Lever, A. B. P. *Inorg. Chem.* **1990**, *29*, 1271.

Table 3. Bond Distances (Å) and Bond Angle Terms (deg) for *trans*-Cr(RIDA)₂ Complexes


ligand	Cr–N	Cr–O _A	Cr–O _B	Δ(Cr–O _A –C) ^a	Δ(Cr–O _B –C) ^a	Σ(ΔO _i) ^b	Σ(ΔN) ^c
<i>i</i> -PIDA ^d	2.118	1.972	1.956	5.7	7.4	77.2	22.8
<i>t</i> -BIDA ^e	2.152	1.974	1.953	6.7	8.4	83.6	28.7

^a Δ(Cr–O_A–C) and Δ(Cr–O_B–C) are deviations of the individual Cr–O–C bond angles from 109.5°. ^b Σ(ΔO_i) is the sum of the absolute deviations of the 12 O–Cr–O and O–Cr–N bite angles from 90°. ^c Σ(ΔN) is the sum of the absolute deviations of the six bond angles made by each nitrogen atom from 109.5°. ^d Reference 27. ^e Reference 28.

theory applied to electrode reactions⁴⁹ the difference in inner-shell barrier heights can be estimated from the following expression:⁵⁰

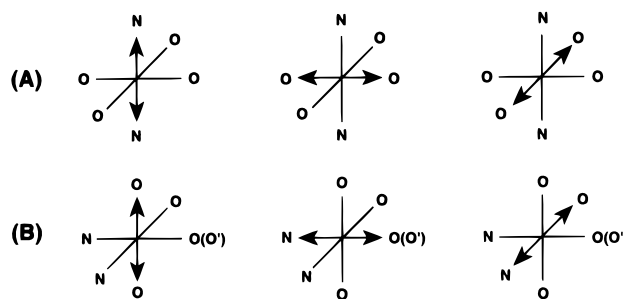
$$\Delta(\Delta G_{is}^\ddagger) = -RT \ln[k_{s,h}(\text{RIDA})/k_{s,h}(\text{IDA})] \quad (11)$$

We measure rate constant ratios of 0.01 and 0.05 for the MIDA and EIDA complexes, respectively, which leads to estimated inner-shell barrier height differences of 11.4 and 7.4 kJ mol⁻¹ for the methyl and ethyl derivatives relative to Cr(IDA)₂⁻.

The inner-shell distortions that accompany Cr(RIDA)₂⁻ reduction also produce a second difference in electrochemical behavior. There is no evidence of chemical reactivity associated with the electrochemistry of *cis*-N₂O₄ species. However, reduction and reoxidation of Cr centers with *trans* N donors are accompanied by displacement and reattachment of a bound carboxylate group. Simulation of the entire reaction sequence (Figure 4) indicates that carboxylate attachment is favored in the chromium(III) oxidation state ($K_{\text{III}} \approx 100$) and that carboxylate displacement is favored in chromium (II) ($1/K_{\text{II}} \approx 20$). The rate constants of these reactions are larger for the chromium-(II) oxidation state, consistent with the greater kinetic lability of Cr²⁺ versus Cr³⁺. The magnitudes of K_{III} and K_{II} are such that *trans*-Cr^{III}N₂O₃O' species are not detected at equilibrium on initial voltammetric scans and *trans*-Cr^{II}N₂O₄ species are not detected on reverse voltammetric scans under the conditions of our experiments.

There are several pieces of evidence which support the interpretation that the chemical reactions in Figure 2 involve exchange of aquo and carboxylate ligands. First, the formal potential of the couple generated by reduction and rearrangement of *trans*-Cr^{III}(RIDA)₂⁻ is consistent with the $E_2^{o'}$ of complexes containing an N₂O₃O' donor atom set (Table 1). Second, Cr–carboxylate bond cleavage is anticipated because Cr–N bonds are kinetically inert. Third, the rate constants for reattachment of the pendant carboxylate group to Cr(III) ($k_{\text{III,on}}$, Table 2) are of the same order of magnitude as those involving chelate ring closure in Cr(EDTA)(H₂O)₂⁻ and related species.^{33a} Finally, we note from the data in Table 2 and the qualitative behavior of the *n*-PIDA and *n*-BIDA complexes that ($k_{s,h}$)₁, $k_{\text{II,off}}$, and $k_{\text{III,on}}$ all increase in the sequence MIDA < EIDA < *n*-PIDA < *n*-BIDA. Thus, the kinetics of Cr^{III/II} electron transfer and of chemical reactions at the Cr center appear to increase systematically with alkyl chain length.

What are the reasons for the difference in behavior exhibited by the *trans*-Cr(RIDA)₂⁻ and *cis*-Cr(IDA)₂⁻ complexes? We believe that a plausible explanation derives from the differences

**Figure 5.** Jahn–Teller distortions in (A) *trans*- and (B) *cis*-N₂O₄ coordination environments.

in ground state structures of these species and the effect of Jahn–Teller distortions experienced upon reduction to the chromium(II) oxidation state. A simple representation of the tetragonal elongations experienced by *trans*-N₂O₄ and *cis*-N₂O₄ coordination environments is given in Figure 5. An important factor is the unique distortion that results in simultaneous elongation of two Cr–N bonds in the *trans*-Cr^{II}N₂O₄ structure (Figure 5a). Table 3 contains X-ray structural data for the R = isopropyl and *tert*-butyl derivatives of Cr(RIDA)₂⁻. Included there are Cr–N and Cr–O bond distances and angular terms that are indicative of strain in the chelate rings.⁵¹ Table 3 shows that the Cr–N distance lengthens as the size of the *N*-alkyl substituent on the iminodiacetate ligand increases. This displacement approximates the Cr–N bond lengthening that would occur via Jahn–Teller distortion along the N–Cr–N axis upon reduction to Cr(II). Concomitant with this chromium–nitrogen bond elongation is an increase in strain in the two glycinate rings of each facially coordinated RIDA ligand; this is indicated by the increases in the Σ(ΔO_i) and Σ(ΔN) parameters in Table 3. The principal structural changes contributing to these terms are reduction of the O–Cr–N bite angles and distortion of the Cr–N–C bond angles.

The data in Table 3 suggest that *trans* N–Cr–N bond lengthening creates strain simultaneously in all four chelate rings of the coordinated RIDA molecules. In effect, each ligand is forced away from the metal by elongation of the bond to the central donor atom. These distortions contribute to the inner-shell part of the Cr(RIDA)₂⁻²⁻ electron transfer barrier and facilitate Cr–carboxylate bond cleavage following reduction. Thus, as the Cr^{III}–N distance in the ground state increases, the activation barrier associated with electron transfer is reduced and the Cr–carboxylate bond is weakened. The principle is that differences in ground state structure are an indicator of kinetic reactivity.⁵²

(49) (a) Marcus, R. A. *J. Chem. Phys.* **1965**, *43*, 679. (b) Marcus, R. A. *Electrochim. Acta* **1968**, *13*, 995.

(50) (a) Feng, D.; Schultz, F. A. *Inorg. Chem.* **1988**, *27*, 2144. (b) Zhang, X. L.; Hupp, J. T.; Danzer, G. D. *J. Electroanal. Chem. Interfacial Electrochem.* **1995**, *380*, 229.

(51) Douglas, B. E.; Radanovic, D. J. *Coord. Chem. Rev.* **1993**, *128*, 139.

(52) (a) Bürgi, H. B.; Dunitz, J. D. *Acc. Chem. Res.* **1983**, *16*, 153. (b) Bürgi, H. B. In *Perspectives in Coordination Chemistry*; Williams, A. F., Floriani, C., Merbach, A. E., Eds.; Verlag Chemie: Weinheim, Germany, 1992; pp 1–29.

Jahn–Teller distortions undoubtedly occur in the reduced forms of $\text{Cr}(\text{IDA})_2^-$ and other chromium complexes with *cis*- N_2O_4 and *cis*- $\text{N}_2\text{O}_3\text{O}'$ donor sets. However, the strain produced presumably is less significant in these cases because two Cr–N bonds cannot be stretched simultaneously. Consequently, the $\text{Cr}^{\text{III/II}}$ couples exhibit larger rates of electron transfer and the reduced forms are less susceptible to chemical reaction.

Acknowledgment. Support of this research by the National Science Foundation (F.A.S., Grant CHE-9214748) is gratefully acknowledged. The authors thank Professors David McMillin

and Hans-Beat Bürgi for helpful discussions. M. Boddin is recognized for contributions to the initial stages of the work.

Supporting Information Available: Four tables of electrochemical data (Tables S1–S4) and Figures S1 and S2, illustrating respectively the determination of $(k_{s,h})_1$ and $k_{\text{II,off}}$ from $E_{p/2}$ data by multiparametric fitting and the comparison of experimental and simulated cyclic voltammograms for $\text{Cr}(\text{MIDA})_2^-$ reduction (6 pages). Ordering information is given on any current masthead page.

IC960152O